Applied Physics A (2018) 124:560
https://doi.org/10.1007/s00339-018-1986-6

Applied Physics A
Materials Science & Processing

Spatio-temporal dynamics of femtosecond laser pulses at 1550 nm wavelength in crystal silicon

Viktor Kadan[1] · Svitlana Pavlova[1] · Ihor Pavlov[1,2] · Hossein Rezaei[2] · Ömer Ilday[2,3,4] · Ivan Blonskyi[1]

Received: 10 January 2018 / Accepted: 19 July 2018 / Published online: 23 July 2018

Abstract
Spatio-temporal transformation of the femtosecond laser pulses at 1550 nm wavelength in c-Si is observed using the methods of time-resolved microscopy. The temporal dynamics of the pulse manifests itself both in widening of the frequency spectrum and in the change of on-axis time-width. It is shown, that along with Kerr effect, two-photon absorption also contributes to the temporal reshaping of the laser pulse. Despite the fact that absorption length for green light in c-Si is as small as 1 μm, generation of visible third harmonics was also observed in c-Si.

1 Introduction

Special properties of femtosecond (fs) laser pulses, such as ultrashort temporal width and, consequently, ultrahigh power, make them an attractive instrument for micromachining and micro-modification of photonics materials, among which perhaps, crystal silicon (c-Si) is the most important. Nowadays, the most widespread 800-nm fs laser pulses are well suited for the processes, which are based on strong surface absorption, e.g., surface ablation for micromachining. On the other hand, material transparency is required for production of embedded microoptical elements, such as waveguides, Y-splitters, combiners, diffractive elements, etc., because it requires precise local energy deposition into the bulk of the material. Therefore, for local modification of optical properties inside the c-Si bulk, fs laser with longer wavelength, e.g., 1550 nm, should be used. Indeed, in [1], we for the first time reported 1550-nm fs laser writing of waveguides deeply embedded in c-Si. However, peculiarities of propagation and spatio-temporal transformation of 1550-nm fs laser pulses in c-Si are still poorly understood, though their knowledge is strongly needed for optimization of the process of fs laser modification. Propagation of the fs laser pulses at 1.55 μm wavelength in c-Si was studied in [2] the regime of strong TPA. Interaction of fs laser pulses at 1200 nm wavelength with c-Si was reported in [3, 4]. However, much more sophisticated equipment is required for generation of the fs laser pulses at 1200 nm, than at 1550-nm, and therefore, 1550-nm fs lasers are more valuable for technological applications. Appropriate methodologies are needed to study the propagation of ultra-short laser pulses in c-Si, because the finite mobility of charge carriers in electronic detectors limits their response time, thus making them too slow for time-resolved studies of ultrafast processes.

In this paper, we present the results of experimental study of spectral and spatio-temporal transformation of femtosecond laser pulses at 1550 nm wavelength in c-Si. First, spectral transformation of the laser pulse has been revealed, which manifests itself in widening of the pulse spectral band and generation of third harmonic (THG). Second, to perform this study, two important methodological tasks have been resolved. We developed and built fs fiber laser, providing output pulses of $M^2 = 1.5$ at 1550 nm wavelength with up to 2 μJ energy and up to 1 MHz repetition rate. Earlier, more simple design of the fs fiber laser at 1550 nm was reported in [5]. The details of the present design will be reported elsewhere. With this laser as a beam source, we designed and built a pump–probe microscopy setup, working both in bright-field and cross-polarized light illumination mode at 1550 nm wavelength. Finally, using the pump–probe setup, we recorded instantaneous polarized light microscopic

✉ Viktor Kadan
vikkadan@yahoo.com; kadan@iop.kiev.ua

[1] Institute of Physics of the NAS of Ukraine, Prospect Nauky 46, Kyiv 03680, Ukraine

[2] Department of Physics, Bilkent University, Ankara, Turkey

[3] Department of Electrical and Electronics Engineering, Bilkent University, 06800 Ankara, Turkey

[4] UNAM, National Nanotechnology Research Center and Institute of Materials Science and Nanotechnology, Bilkent University, 06800 Ankara, Turkey

pictures of spatio-temporal transformation of the laser pulse itself, propagating inside c-Si plate at 1550 nm wavelength. Under the bright-field illumination, the resulting picture is formed by interplay of TPA and Kerr- and plasma-induced modifications of refractive index. Both bright-field and cross-polarized microscopy reveal temporal widening of the propagating pump pulse, which at least partially, can be caused by TPA.

2 Experimental

Self-made fiber laser, consisting of oscillator and two amplifiers, produces a train of light pulses with up to 2 μJ energy, which repetition rate can be set from 100 kHz up to 1 MHz. The central wavelength of the pulses is 1.55 μm, their time-width Δt_p is 400–450 fs. Using the above laser as a light source, experimental setup of time-resolved microscopy has been built, capable to visualize the propagation of 1550-nm fs laser pulses in c-Si (Fig. 1). The setup can easily be switched from cross-polarized to bright-field illumination by rotating the polarizing cube P3. Note, that while the strong emission at 1200 nm can still be recorded with Si-based CCD-camera taking advantage of the residual absorption tail in Si (see e.g., [4]), InGaAs-based IR camera is needed to record the 1550-nm emission. Therefore, we used InGaAs camera in our setup, which, with matrix of 640 × 510 pixels and 10× microscopic objective MO provides resolution of 3.6 μm/pix. The temporal delay τ between the pump and probe pulses can be changed with a delay line DL, thus making possible to recover the time-resolved dynamics of the process under study. In the mode of polarized light microscopy, the probe light does not pass the crossed polarizers P3 and P4, each of them being set at the angle of 45° to the polarization plane of the pump beam. In such a case, the microscope image field is completely dark. However, strong electric field of the pump pulse induces a transient birefringence in c-Si sample through fast electronic Kerr effect with response time about 1 fs. As a result, induced birefringence area appears, which moves together with the pump pulse. Acting as a transient retarder plate, it induces ellipticity in originally plane polarization of the probe pulse, thus allowing part of the probe light to pass the polarizer P4 and form the instant picture of the pump pulse. Note, that laser-induced plasma, though changing the refractive index, does not form the picture under the cross-polarized light illumination because the plasma-induced change is not birefringent. If the Kerr-induced phase shifts are small, the intensity of the signal I_{POL}, is described by the formula [6]:

$$I_{POL} = \pi^2 l^2 n_2^2 I_p^2 I_{probe} / \lambda_{probe}^2, \quad (1)$$

where l is the the intersection length of the pump and probe pulses, n_2 is the nonlinear refractive index, I_p is the intensity of the pump light, I_{probe} is the intensity of the probe light, and λ_{probe} is the probe wavelength. If the axes of the polarizers are set in parallel, the camera records instant bright-field transmission picture of the probe pulse.

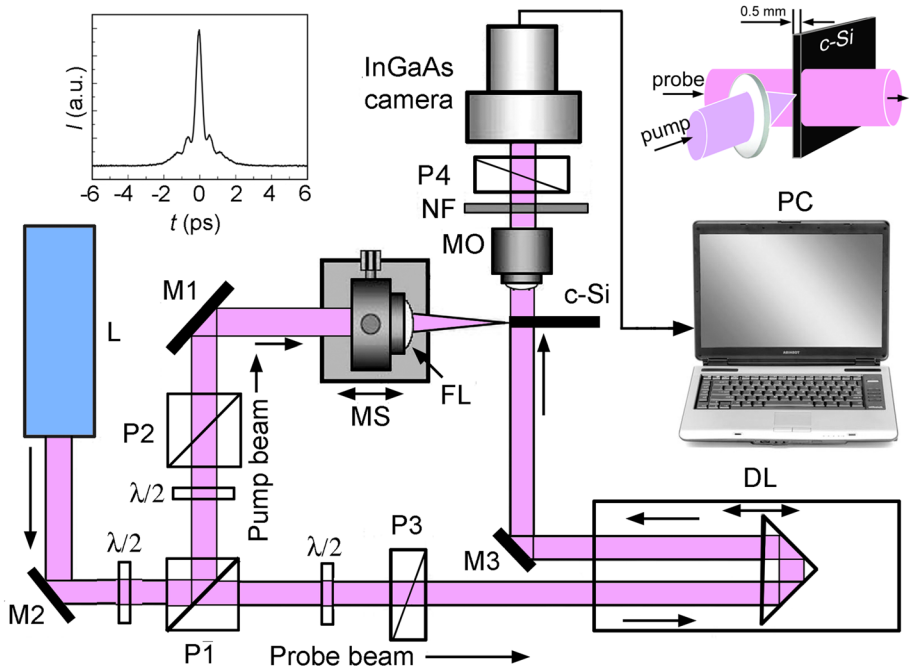

Fig. 1 Pump–probe microscopy setup. The focus of the pump light is on the front face of c-Si crystal as shown in the upper right inset, which schematically illustrates the pump–probe configuration. The focusing lens FL with 35 mm focal distance provides the focal spot of 24 μm diameter and Rayleigh length 1200 μm. The upper left inset shows autocorrelation trace of the output laser pulses of 2 μJ energy at 250 kHz repetition rate

3 Spectral transformation of the fs laser pulses at 1550 nm in c-Si

In the following experiment, the laser pulses of different energies E_p up to 1.3 μJ at 1.55 μm wavelength with repetition rate $f = 250$ kHz, and temporal width $\Delta t_p = 450$ fs were focused with aspherical lens L of 35 mm focal distance in such a way that the beam waist of 24 μm diameter and 1200 μm Rayleigh length was on the front face a 0.5 mm-thick c-Si plate, as shown in Fig. 2b. We measured IR (1400–1700 nm) and visible (500–530 nm) spectra of the transmitted radiation. Original spectrum of the laser light is shown in Fig. 2a, and transmitted IR spectra at two pulse energies $E_p = 8$ nJ and $E_p = 1.3$ μJ—in Fig. 2c, d correspondingly. Taking into account that according to [2], the laser pulse of the energy $E_p = 70$ nJ with $\lambda_p = 1.55$ μm and $\Delta t_p = 100$ fs in c-Si has the power of 24 critical energies of self-focusing P_{crit}, we assume that in our case, the critical power of self-focusing for the pulse of temporal width $\Delta t_p = 450$ fs corresponds to the pulse energy $E_p = 12$ nJ. Proceeding from this, and also from the fact that the widths of the spectral bands in Fig. 2a, c are the same, we conclude that the propagation mode in Fig. 2c is linear, and in Fig. 2d—highly nonlinear with $P \approx 100\, P_{crit}$.

The comparison of Fig. 2a, c, d reveals significant temporal dynamics of the fs laser pulse in nonlinear propagation mode at $E_p = 1.3$ μJ, which manifests itself as a widening of the output IR spectrum in Fig. 2d. The widening is more appreciable at the band wings, while around the band maximum it is weaker. Indeed, at the level of 10^{-3}, the band width increases from 50 to 100 nm. We believe that the observed spectral widening is due to the time-dependent nonlinear change of the refractive index $n_2 I(t)$ which causes the phase change and consequently, the frequency shift $\Delta\omega(t)$ of the input spectral band as a result of self-phase modulation (SPM). In the case of the flat-wave and Kerr nonlinearity [7]

$$\Delta\omega(t) = -\frac{n_2\omega_0 z}{c}\frac{\partial I(t)}{\partial t}. \tag{2}$$

Typically, for positive n_2, the rising edge of the pulse shifts the frequency to the red side, while the sloping edge produces the blue shift. For a Gaussian temporal pulse shape the blue- and red frequency shifts should be the same. However, the plasma of free carriers of density N_e, excited in the process of two-photon absorption (TPA), influences the SPM through the plasma-caused decrease of the refractive index, given by $\Delta n = -N_e/2n_0N_{cr}$, if the critical plasma density $N_{cr} > N_e$. Thus, disregarding recombination of carriers for as long as the pulse lasts, the plasma causes only blue frequency shift according to the expression [8]:

$$\Delta\omega(t) \approx \frac{\omega_0 z}{2cn_0N_{cr}}\frac{\partial N_e(t)}{\partial t}. \tag{3}$$

However, due to nonlinearity of SPM, only a part of the total pulse energy located around the high-intensity axis undergoes the main frequency shift. The intensity profile of this part is described by the square of Gaussian function

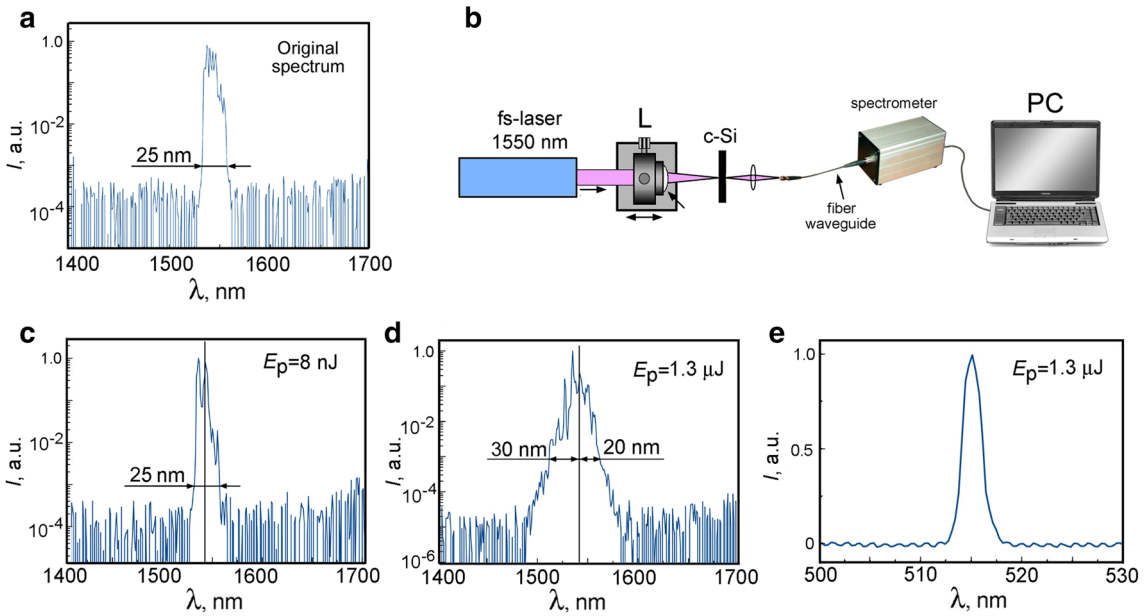

Fig. 2 Original spectrum of the laser pulses (**a**). Configuration of the measurements (**b**). IR spectra of the laser pulses, exiting the 0.5 mm-thick c-Si plate at the input pulse energies $E_p = 8$ nJ (**c**) and $E_p = 1.3$ μJ (**d**). Visible output spectrum at $E_p = 1.3$ μJ (**e**)

for Kerr-induced- and by the cube—for plasma-induced SPM, i.e., it is correspondingly, 1.4- and 1.7 times narrower than the original Gaussian waist. Thus, the spectral widening of the total pulse, whose transversal intensity profile is described by a Gaussian function, becomes more evident at the level of low-intensity wings. Note, that we have measured the spectrum of the total pulse, including the core and periphery. In Fig. 2d, the stronger shift of the spectrum toward the higher frequencies, measured at the level 10^{-3}, indicates the influence of the plasma of free carriers on the SPM. Assuming, that the Kerr-induced blue- and red frequency shifts are 7.5 nm each, we conclude, that the additional frequency shift of 10 nm to the blue side is caused by the laser-induced plasma. Thus, the SPM, manifesting itself as blue- and red spectral shifts, is an attribute of nonlinear temporal dynamics in the propagating pulse.

4 Third harmonic generation by the fs laser pulses at 1550 nm in c-Si

The next unexpected phenomenon of the pulse frequency transformation, which we observed in c-Si under the above parameters of the fs laser excitation, is the generation of third harmonic (THG). The experimental scheme is shown schematically in Fig. 3a. The lens L with focal distance of 35 mm provides diffraction-limited diameter of the focal spot 24 μm at FWHM and Rayleigh length 1200 μm. When the focal spot is close to the output face of the 0.5-mm-thick c-Si plate, a green light beam appears at E_p ranging from 400 nJ to 1.3 μJ, bright enough to be visible by the naked eye in the dark room. It propagates coaxially with the pump beam of $\lambda_p = 1550$ nm wavelength.

According to the spectral measurements (Fig. 2e), the green emission wavelength is centered at $\lambda_{TH} = 516$ nm, suggesting its origin as third harmonics of the pump laser band. The fact is rather surprising, because the absorption length in c-Si at $\lambda = 516$ nm is only 1 μm. Note, that THG is one of a few processes, allowing emission of visible light from Si. Visible luminescence is known from nanostructured, particularly porous Si [9]. THG in c-Si in UV under 1.06 μm picosecond excitation has been detected in early work [10]. THG in silicon-based materials was observed in silicon nanoparticles [11]. TH was also generated in photonic crystal waveguides as a result of spatial pulse compression involving the slow light phenomenon [12, 13]. However, as far as we know, reports on THG in bulk c-Si at $\lambda_p = 1550$ nm, visible by naked eye, are missing, despite the fact that THG in this material is an allowed process, in which third-order nonlinear polarization $\mathbf{P}^{(3)}(3\omega)$ at the tripled frequency is given by [7]: $\mathbf{P}^{(3)}(3\omega) = \chi^{(3)}(3\omega = \omega + \omega + \omega)$:$\mathbf{E}(\omega)$ $\mathbf{E}(\omega)$ $\mathbf{E}(\omega)$, where $\chi^{(3)}$ is the nonlinear susceptibility of the third order.

Next, we estimate the fulfillment of wave-vector matching conditions in the THG process. Absorption coefficient of c-Si at $\lambda_{TH} = 515$ nm is 1×10^4 cm^{-1}. It determines the effective interaction length $l^* = 1$ μm for the TH emission in c-Si. At the same time, in plane-wave approximation, the wave-vector mismatch $\Delta\mathbf{k} = \mathbf{k}_s - 3\mathbf{k}_0$ is 8.5 μm^{-1}. The coherence length for THG at such $\Delta\mathbf{k}$ is 0.37 μm. Thus, the mismatch reduces the intensity of the matched THG signal by the factor η [14], which depends on the scalar product of two vectors:

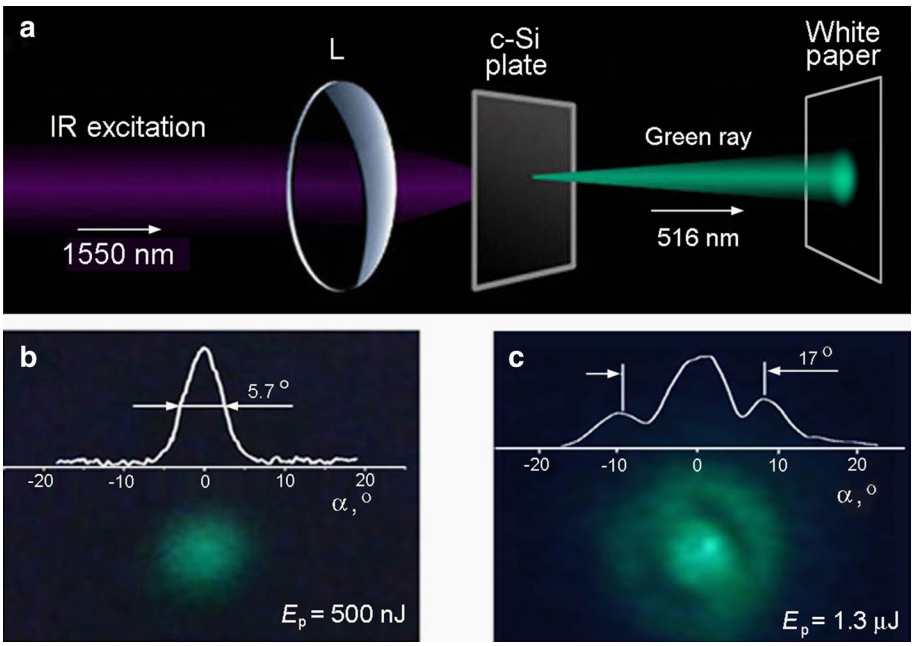

Fig. 3 THG in c-Si. Experimental scheme (**a**). Picture and angular profile of the TH beam generated in 0.5-mm-thick c-Si plate at $E_p = 500$ nJ (**b**). Picture and angular profile of the TH beam generated in 8-mm-thick c-Si plate at $E_p = 1.3$ μJ (**c**)

$$\eta = \mathrm{sinc}^2(\Delta\mathbf{k}\mathbf{l}^*/2). \quad (4)$$

Here, $\mathbf{l}^*$ is the vector of interaction length (~ 1 μm for $\lambda_{TH} = 515$ nm). Considering very small interaction length, we should not expect, that condition (4) leads to sharply directional TH emission. Indeed, as follows from formula (4) at $l^* = 1$ μm, $\eta(\alpha) \approx 0.044$. It is practically independent of α in the range $\pm 30°$, where α is the angle of TH emission in air relative to the optical axis. However, the measured angular profile of the TH beam (Fig. 3b, c) is much more directional, as compared with that of $\eta(\alpha)$. The reason for this is phase matching of the transversal components of wave-vectors over the beams' cross-section. In the flat-wave approximation, the transversal mismatch becomes zero if the TH emission propagates collinearly with the pump wave. The pump beam in our case is nearly Gaussian, its diameter at FWHM being 6 mm. For the focal distance of the lens L 35 mm, the width of the angular profile of the pump beam is 10° at FWHM. However, the measured angular profile of TH is only 5.7° at FWHM. This decrease of the angular spread can be understood as a result of coherent emission at three times shorter TH wavelength $\lambda_{TH} = 515$ nm from a coherent source of diffraction-limited diameter formed by a pump emission with wavelength $\lambda_p = 1.55$ μm. The diffraction-limited radius of the waist w_p of the Gaussian pump beam is $w_p = \lambda_p/\pi\theta_p$, where θ_p is a half-angle of the pump beam at $1/e^2$. However, the coherent source at λ_{TH} is formed by nonlinear polarization $\mathbf{P}^{(3)}(3\omega)$. The Gaussian intensity cross-section of this nonlinear source is determined by the third power of the Gaussian profiles of the pump intensity, its waist w_{TH} being by the factor $3^{1/2} = 1.73$ narrower, than that of the pump beam, $w_{TH} = w_p/1.73$. Thus, the width of the resulting diffraction-limited angular profile of the TH beam is defined by two counteracting factors. First, it should be 3 times narrower, than the pump beam, because of the smaller wavelength. Second, it should be 1.73 times wider because of the smaller source waist. Combined action of these two factors results in the actual diffraction-limited angular profile of the TH beam 1.73 times narrower than that of the pump beam, i.e., exactly 5.7° at FWHM, as has been found experimentally for 0.5-mm-thick c-Si sample (Fig. 3b). As will be shown below, and according to [2, 3], at sufficient pulse energy and increased thickness of the c-Si sample, actual shape of the pump beam becomes distorted by TPA and plasma refraction. Indeed, we found, that in 8-mm-thick c-Si sample, where the shape of the pump beam, focused on the exit face of the sample, is surely not Gaussian, the profile of TH emission acquires a ring component (Fig. 3c).

Addressing the role of the surface in THG, which along with the bulk, contributes to the total TH signal, it is expected that the bulk and surface contributions are roughly related as l/a, where l is the shorter of the coherence and absorption lengths, and a is the lattice constant [15, 16]. As already mentioned above, for excitation at 1.55 μm in c-Si, the coherence length for THG is 0.37 μm, absorption length for TH wavelength is 1 μm, while the lattice constant $a = 0.54$ nm. Therefore, the bulk should provide a dominant contribution to THG. Moreover, despite the conclusions of [17, 18] about the strong enhancement of the surface contribution to THG in transparent materials, the experiments [16] on the THG by Ti:sapphire femtosecond laser with central wavelength 820 nm in thin c-Si wedges, demonstrate a negligible surface contribution. Considering that under the Ti:sapphire laser excitation, the absorption length for TH $\alpha^{-1} = 4.5$ nm is much smaller than the coherence and absorption lengths under 1.55-μm excitation, these results, though obtained for different wavelength, strongly suggest that the volume contribution to THG also dominates under the 1.55-μm excitation.

5 Time-resolved spatio-temporal evolution of the propagating fs laser pulse

The next experiment has been performed using the time-resolved microscopy setup, shown in Fig. 1. It visualizes the spatio-temporal transformation of the 1.55-μm fs laser pulse propagating in 0.5-mm-thick c-Si plate and the TPA-generated plasma tail which follows the laser pulse. In the experiment, the laser pulses of energy $E_p = 1.14$ μJ and repetition rate $f = 250$ kHz were focused on the entrance face of the c-Si crystal as shown in the upper right inset in Fig. 1. As far as we know, this is the first use of time-resolved microscopy for observation of spatio-temporal transformation of the 1.55 μm laser pulses propagating in c-Si.

The instant pictures obtained in cross-polarized illumination mode are shown in Fig. 4a. For better visual perception, they are presented in negative, so that darker areas represent more intense transmitted light. In fact, these darker spots depict the laser pulse itself, which becomes visible due to the instant light-induced birefringence. The time delay τ between the pump and probe pulses in picoseconds is indicated at the upper right corner of each panel. Since τ is a relative value, it is assumed that the pulse position on the left edge of the panel corresponds to zero delay both for bright-field and cross-polarized illumination. Considering, that the refractive index n in c-Si is 3.48 at 1.55 μm, the propagation velocity of the pulse maxima in Fig. 4a correspond to the light speed in the material. The diameter at FWHM of the transversal intensity profile of the signal I_{POL} at cross-polarized illumination in Fig. 4a is 18 μm at $\tau = 0.61$ ps. Taking into account the quadratic dependence of I_{POL} on the pump intensity I_p according the formula (1), we get, that the diameter at FWHM of the transversal intensity profile of the pump beam is 25 μm. This value agrees well with the diffraction-limited diameter of the laser focal spot $d = 24$ μm.

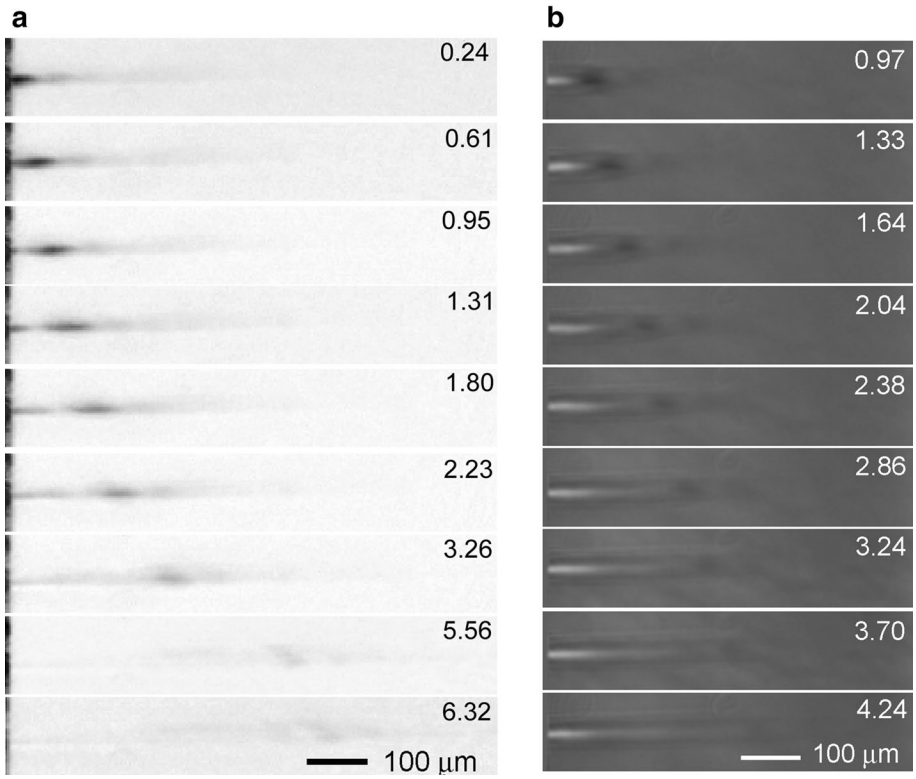

Fig. 4 Laser pulses propagating in 0.5-mm-thick c-Si sample under the fs excitation at the 1550 nm wavelength, $f = 250$ kHz repetition rate and single-pulse energy $E_p = 1.14$ μJ. The time delays τ in picoseconds are indicated at the upper right corner of each panel. Polarized light microscopy (**a**). Bright-field microscopy (**b**)

Apart from the main pulse, smaller satellite pulses ahead of- and lagging behind the main pulse are visible at ~ 0.7 ps. They are caused by non-ideal temporal profile of the laser pulse (see the autocorrelation trace inserted in Fig. 1). The axial intensity of the pump pulse is maximum at small τ up to 0.95 ps, while at longer time delays it decreases, and starting from $\tau = 3.26$ ps, transversal pulse splitting becomes perceptible.

To reveal the evolution of the time-width Δt of the laser pulses while propagating inside the c-Si sample, we measured their axial intensity profiles at different τ. The measurement procedure illustrated in Fig. 5a by an example of the picture fragment, taken from Fig. 4a ($\tau = 0.95$ ps), was carried out using public domain Java image processing program ImageJ 1.47 v. The program builds the gray level profile along the selected plot, which in Fig. 5a is shown by white rectangle. The width of the profile at FWHM divided by the light speed in c-Si represents the temporal width Δt of the axial part of the pulse at $\tau = 0.95$ ps. To find if the shape of the selection influences the measured FWHM of

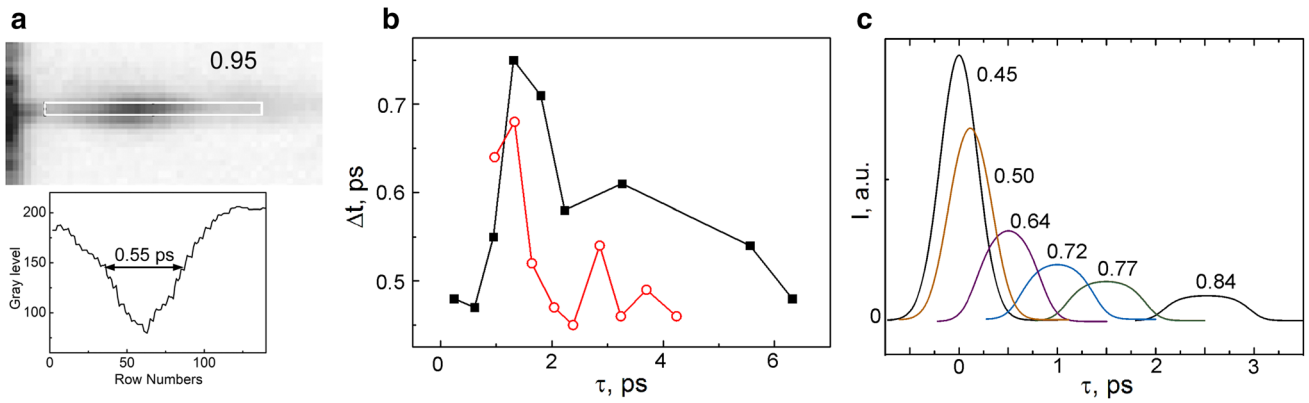

Fig. 5 The procedure of measurement of Δt (**a**). On-axis temporal width Δt at FWHM of the laser pulses in c-Si, depending on the time delay τ between the pump and probe pulses (after the data of polarized light- (solid squares) and bright-field (open circles) microscopy). The lines are added to guide the eye (**b**). Calculated dependence of the TPA-induced transformation of the pulse temporal shape on τ (c). The FWHM of the pulse in picoseconds is indicated at every curve

the gray level profile (Δt), we tried the selections of different height. It has been established that the measured Δt is almost insensitive of the selection height, the variations not exceeding 10%. We believe that this is a sufficient precision for qualitative interpretation of the following results.

The plot of $\Delta t(\tau)$ basing on the pictures presented in Fig. 4a is shown by solid squares in Fig. 5b. It should be noted, that while average Δt is consistent with the temporal width of the laser pulse $\Delta t_p = 450$ fs, a noticeable increase of the axial pulse duration up to 0.75 ps occurs at τ 1.31 and 1.80 ps.

The bright-field microscopic pictures are presented in Fig. 4b. Plasma of free carriers generated by the pump beam through TPA, forms the tail, which follows the propagating laser pulse in Fig. 4b. Due to the plasma-caused negative change of the refractive index, the plasma tail refracts the probe light as a concave cylindrical lens, thus becoming visible at small defocusing of the object plane of the microscope (200 μm beneath the actual plasma tail in Fig. 4b). We have found that the plasma-caused tail keeps unchanged for several nanoseconds in agreement with the free carrier lifetime of more than 10 ns in c-Si, but completely disappears if the pump light is turned off. At zero defocusing, the plasma tail is almost invisible, indicating that plasma absorption through inverse bremsstrahlung is much weaker than TPA. The TPA involving one pump- and one probe photon is visualized as a dark spot ahead of plasma tail, which moves to the right at the increase of τ. Similar to Kerr effect, the response time of TPA is also of the order of femtoseconds [19]. Thus, the pulse temporal width can be also estimated from the bright-field pictures using the same procedure, as for cross-polarized illumination. Similar to Fig. 4a, the propagation velocity of the TPA maximum is defined by the velocity of light in c-Si. Open circles in Fig. 5b present the temporal width Δt at FWHM of the on-axis longitudinal intensity profiles of TPA at differentτ. The average width Δt is consistent with the duration of the laser pulse. It is also evident, that the axial pulse width significantly exceeds the width of the laser pulse $\Delta t_p = 450$ fs at the τ ranging from 0.97 to 1.33 ps, reaching 0.68 ps. Taking into account possible uncertainty in defining the moment of zero delay, and defocusing of 200 μm in Fig. 4b, we conclude, that at present experimental conditions, the time-width of the axial part of the pump pulse increases from 450 to ~ 700 fs at τ ~ 1.3 ps.

Note, that the increase of Δt of the on-axis part of the pulse, recorded both in bright-field- and polarized light microscopy, cannot be attributed to the linear dispersion in silicon, which broadens the input 100 fs pulse to 265 fs in 8 mm propagation according to [2]. Considering the subsequent pulse narrowing at longerτ, the maximum propagation distance that is only 0.6 mm in Fig. 4, and that the transform-limited frequency band of 450-fs pulse is 4.5 times narrower than the band of 100-fs pulse, we can neglect the influence of the linear dispersion on the observed pulse broadening in our measurements. Thus, the observed pulse broadening unambiguously indicates the presence of nonlinear temporal dynamics. Nonlinear temporal broadening and splitting of ultrashort laser pulses is well known in wide-gap dielectrics. It is found [20, 21], that one of the main physical mechanisms of this phenomenon is SPM, which "expels" the frequency-shifted components of the pulse forward and backward from the pulse maximum due to the dispersion of the group velocity. However, we believe, that in narrow-gap semiconductors, such as c-Si, TPA at least partially is responsible for the pulse broadening, flattening the more intensive top of the pulse.

It should be taken into account, that the pictures in Fig. 4b apart from TPA, are formed by Kerr-induced positive- and plasma-induced negative transient change of the refractive index. All these factors contribute to the nonlinear dynamics of the propagating fs laser pulse in Kerr dielectrics, where balance between Kerr self-focusing and plasma defocusing leads to the formation of filaments. To enable their formation, the TPA, which hinders self-focusing [22], should be sufficiently low. This implies the requirement $K \geq 3$, where K is the nearest integer of $[E_g/h\nu_{pump}]$ [21]. However, in c-Si the TPA becomes one of dominant factor, defining nonlinear dynamics of the pulse propagation. Partially this issue has already been considered in the literature. In [3] refraction on the TPA-generated plasma was supposed to be the main factor changing the spatial shape of the fs laser pulses at 1.2 μm in c-Si. The authors of [2] introduced three parameters—diffraction-, TPA- and Kerr length, interplay of which defines the fs pulse transformation in c-Si. Using the above-mentioned pulse parameters and assuming the diffraction-limited diameter of the laser focal spot $d = 24$ μm, we estimated the transient absorption, induced by the pump pulse through the TPA process. The coefficient of TPA is taken as $\beta_{TPA} = 4 \times 10^{-6}$ μm/W [23]. According to the estimation, the presence of the above laser pulse induces in c-Si the linear absorption value $\alpha_{ind} = \beta_{TPA} I = 4.5 \times 10^{-2}$ μm^{-1}, which qualitatively agrees with the profiles of transient absorption in Fig. 4b.

Further, we draw attention to the fact, which, to our knowledge, is insufficiently covered in the literature. Being a nonlinear process, the TPA flattens not only transversal distribution of the pulse intensity but also its shape along the propagation axis, thus increasing the pulse time-width. To illustrate qualitatively the role of TPA in changing the pulse temporal width and amplitude, we made the following estimation. Assuming that due to TPA, the intensity $I(t,\tau)$ of the laser pulse traveling inside c-Si for a period of time τ diminishes as:

$$I(t,\tau) = \frac{I_0(t)}{1 + I_0(t)\beta\tau c/n}, \quad (5)$$

where $\tau c/n$ is the length of beam path inside the material at the time delay τ, and assuming the originally Gaussian temporal shape of the 0.45 ps-long input pulse

$$I_0(t) = I_{\max} e^{-13.7t^2},$$

where t is in picoseconds, we have calculated the TPA-driven evolution of the temporal shape of the pulse $I(t,\tau)$ on the axis at $\beta = 4 \times 10^{-6}$ μm/W and $I_{\max} = 1.13 \times 10^4$ W/μm^2 (see Fig. 5c). Indeed the calculation is qualitatively consistent with the increase of the pulse duration and the decrease of its amplitude observed with polarized light microscopy (Figs. 4a, 5b) at τ ranging from 0 to 1.5 ps. Note, that apart from the temporal widening of the pulse, TPA also changes its transversal distribution, flattening the beam top on the axis, while Kerr self-focusing acts in the opposite direction.

However, the pulse restores its initial time-width with further propagation, as can be seen from Figs. 4 and 5b. One possible explanation of such behavior is that TPA, together with other factors, such as Kerr self-focusing, plasma refraction and absorption, lead to a complex transformation of the pulse, which is manifested as formation of conical Bessel waves [2, 3]. The Bessel waves restore the original on-axis pulse time-width, because they form the energy flux directed on the axis from the surrounding lower-intensity areas, which have not undergone the temporal changes. Moreover, plasma defocusing and absorption through inverse bremsstrahlung act predominantly on the trailing part of the pulse and can thus cause shortening of the axial component of the pulse after initial elongation.

Thus, the evidences of temporal dynamics in the fs laser pulse of 1550 nm wavelength propagating in c-Si have been found both in space and frequency domains. However, the authors of [2] did not find any nonlinear change of the time-width of femtosecond laser pulses at 1.55 μm wavelength with $P = 24\ P_{\text{crit}}$ in c-Si. We believe that there is no contradiction between our conclusion and that of [2]. Apart from the four times lower pulse power and more loose focusing, the authors of [2] tried to find the change of time-width of the on-axis output pulse which had passed 8-mm-thick c-Si slab, while we have found, that the on-axis part of the pulse increases the temporal width on the first 200 μm of the beam path, then recovering its original value.

Finally, tighter beam focusing with the lens of 9 mm focal distance causes irreversible changes of the refractive index of the material in the focal spot. As has been mentioned above, in this way we created permanent built-in waveguides deep in the bulk of c-Si [1], which could find applications in integrated silicon photonics.

Summarizing, temporal dynamics of the fs laser pulse at 1550 nm propagating in c-Si has been for the first time recorded using methods of time-resolved microscopy. It is suggested that TPA is the main factor responsible for the increase of on-axis time-width of the laser pulse during the first 1.5 ps of its propagation. In frequency domain, the temporal dynamics manifests itself as Kerr- and plasma-induced SPM, which non-symmetrically widens the frequency band of the laser pulse. THG, visible by the naked eye has also been observed in c-Si, despite very small absorption length at 516 nm.

Acknowledgements We acknowledge support from the NAS of Ukraine and the Scientific and Technological Research Council of Turkey (TUBITAK) (a joint research project 114F256), Ukrainian State Fund for Fundamental Research (Project F73/23805), as well as from the Science and Technology Center in Ukraine (Project 6174).

References

1. O. Pavlov, S. Tokel, V. Pavlova, G. Kadan, A. Makey, Ö Turnali, Yavuz, F. Ilday, Opt. Lett. **42**(15), 3028 (2017)
2. D. Faccio, M. Clerici, A. Averchi, O. Jedrkiewicz, S. Tzortzakis, D.G. Papazoglou, F. Bragheri, L. Tartara, A. Trita, S. Henin, I. Cristiani, A. Couairon, P. Di Trapani, Opt. Express **16**(11), 8213 (2008)
3. V.V. Kononenko, E.V. Zavedeev, V.M. Gololobov, Appl. Phys. A **122**(4), 293 (2016)
4. V.V. Kononenko, V.V. Konov, E.M. Dianov, Opt. Lett. **37**(16), 3369 (2012)
5. I. Pavlov, E. Ilbey, E. Dülgergil, A. Bayri, F. Ilday, Opt. Express **20**(9), 9471 (2012)
6. J. Takeda, K. Nakajima, S. Kurita, S. Tomimoto, S. Saito, T. Suemoto, Phys. Rev. B **62**(15), 10083 (2000)
7. Y.R. Shen, *The principles of nonlinear optics* (Wiley, New York, 1984)
8. B.M. Penetrante, J.N. Bardsley, W.M. Wood, C.W. Siders, M.C. Downer, J. Opt. Soc. Am. B 9(11), 2032 (1992)
9. L.T. Canham, Appl. Phys. Lett. **57**(10), 1046 (1990)
10. W.K. Burns, K. Bloembergen, Phys. Rev. B **4**(10), 3437 (1971)
11. M.R. Shcherbakov, Nano Lett. **14**(11), 6488 (2014)
12. S. Sederberg, A.Y. Elezzabi, Phys. Rev. Lett. **114**(22), 227401 (2015)
13. B. Corcoran, C. Monat, C. Grillet, D.J. Moss, B.J. Eggleton, T.P. White, L. O'Faolain, T.F. Krauss, Nat. Photon. **3**(4), 206 (2009)
14. S.A. Akhmanov, N.I. Koroteev, *Methods of nonlinear optics in the spectroscopy of light scattering—active spectroscopy of light scattering* (Izdatel'stvo Nauka, Moscow, 1981) **(in Russian)**
15. J.E. Sipe, D.J. Moss, H.M. van Driel, Phys. Rev. B **35**(3), 1129 (1987)
16. P.N. Saeta, N.A. Miller, Appl. Phys. Lett. **79**(11), 2704 (2001)
17. T.Y.F. Tsang, Phys. Rev. A **52**(5), 4116 (1995)
18. T. Tsang, M.A. Krumb ügel, K.W. DeLong, D.N. Fittinghoff, R. Trebino, Opt. Lett. **21**(17), 1381 (1996)
19. Q. Lin, O.J. Painter, G.P. Agrawal, Opt. Express **15**(25), 16604 (2007)
20. J. E. Rothenberg, Opt. Lett. 17(8), 583 (1992)
21. A. Couairon, A. Mysyrowicz, Phys. Rep. **441**(2–4), 47 (2007)
22. S.A. Akhmanov, A.P. Sukhorukov, R.V. Khokhlov, Sov. Phys. Usp. **10**, 609 (1968)
23. J.F. Reintjes, J.C. McGroddy, Phys. Rev. Lett. **30**(19), 901 (1973)